Chemosphere 154 (2016) 444–453

Contents lists available at ScienceDirect

Chemosphere

journal homepage: www.elsevier.com/locate/chemosphere

Fate and transport with material response characterization of green sorption media for copper removal via desorption process

Ni-Bin Chang [a, *], Cameron Houmann [a], Kuen-Song Lin [b], Martin Wanielista [a]

[a] Department of Civil, Environmental, and Construction Engineering, University of Central Florida, Orlando, FL, USA
[b] Department of Chemical Engineering and Materials Science, Yuan Ze University, Taoyuan City 32003, Taiwan, ROC

HIGHLIGHTS

- Multiple cycles of adsorption and desorption confirm that hydrochloric acid has good potential for copper desorption.
- A rapid desorption reaction can be delineated with the Lagergren pseudo-second order model.
- Surface sorption of CuO species is significant in the media mixture and coconut coir.

ARTICLE INFO

Article history:
Received 11 May 2015
Received in revised form
20 March 2016
Accepted 28 March 2016
Available online 12 April 2016

Handling Editor: X. Cao

Keywords:
Adsorption media
Stormwater management
Copper removal
Desorption
Material characterization

ABSTRACT

Multiple adsorption and desorption cycles are required to achieve the reliable operation of copper removal and recovery. A green sorption media mixture composed of recycled tire chunk, expanded clay aggregate, and coconut coir was evaluated in this study for its desorptive characteristics as a companion study of the corresponding adsorption process in an earlier publication. We conducted a screening of potential desorbing agents, batch desorption equilibrium and kinetic studies, and batch tests through 3 adsorption/desorption cycles. The desorbing agent screening revealed that hydrochloric acid has good potential for copper desorption. Equilibrium data fit the Freundlich isotherm, whereas kinetic data had high correlation with the Lagergren pseudo second-order model and revealed a rapid desorption reaction. Batch equilibrium data over 3 adsorption/desorption cycles showed that the coconut coir and media mixture were the most resilient, demonstrating they could be used through 3 or more adsorption/desorption cycles. FE-SEM imaging, XRD, and EDS analyses supported the batch adsorption and desorption results showing significant surface sorption of CuO species in the media mixture and coconut coir, followed by partial desorption using 0.1 M HCl as a desorbing agent.

1. Introduction

Non-point sources of copper loading have impaired a large number of water bodies in the United States by causing copper concentrations in the water column to exceed ambient water quality threshold (US EPA, 2014). Non-point sources include runoff from highways (Davis et al., 2001; Nason and Bloomquist, 2012; Kayhanian et al., 2003; Dean et al., 2005; Hilliges et al., 2013; US EPA, 2014) and agricultural lands (Kayhanian et al., 2003; Graves et al., 2004; Dean et al., 2005; Pitt et al., 2008; Hoang et al., 2009; Nason et al., 2012; Hilliges et al., 2013), and use of copper sulfate ($CuSO_4$) as an algaecide in both natural and manmade water bodies (Chang et al., 2014). The use of green adsorptive filter media, or green adsorption media, to remove copper in stormwater runoff may be regarded as a best management practice (BMP). The term "green" is used here to define media composed of recycled and/or renewable materials; however, once the filter media has reached its adsorptive capacity, it must be replaced and the spent media may need to be disposed as a hazardous waste if copper recovery is not lucrative. To conduct copper recovery, desorption of adsorbed copper has to be achieved through the use of various desorbing agents, primarily acids (Vilar et al., 2007; Singh et al., 2008; Njikam and Schiewer, 2012; Li et al., 2015) and complexing agents (Singh et al., 2008; Njikam and Schiewer, 2012), whose effectiveness may vary between media types, depending on the sorption mechanism involved. Regeneration of the media's sorption sites is important in establishing the media as a cost-effective and sustainable solution for copper removal in stormwater runoff (Tassist

* Corresponding author.
E-mail address: nchang@ucf.edu (N.-B. Chang).

http://dx.doi.org/10.1016/j.chemosphere.2016.03.130
0045-6535/

et al., 2009). The desorbed copper in solution may be removed from the waste stream and recovered using a number of technologies such as reverse osmosis and nanofiltration (Al-Zoubi et al., 2010; Mullett et al., 2014), chemical synthesis (Zhang and Zhang, 2014), precipitation (Xie et al., 2005; Tassist et al., 2009; Chen et al., 2014), and electrolysis (Tassist et al., 2009).

Studies of heavy metal desorption from both green adsorption media and inorganic adsorption media have similar mechanisms (Vilar et al., 2007). Adsorption isotherm equations have been successfully applied to describe equilibrium desorption data, including Langmuir and Freundlich isotherms (Cox et al., 1997; Li et al., 2015), whereas some mechanistic models of desorption equilibrium have been developed (Cox et al., 1997; Vilar et al., 2007; Febrianto et al., 2009; Li et al., 2015). Desorption kinetics have been shown to follow Lagergren pseudo first- and second-order kinetics (Singh et al., 2008; Febrianto et al., 2009; Njikam and Schiewer, 2012) by assuming that the rate of desorption is proportional to the number of metal-filled sites. Adsorption and desorption hysteresis is another phenomenon that has been studied experimentally for sorption media exposed to multiple adsorption/desorption cycles (Cox et al., 1997; Singh et al., 2008; Piwowarczyk and Holden, 2011; Li et al., 2015).

This study aims to evaluate the desorption characteristics of a green sorption media mixture composed of recycled tire rubber, expanded clay aggregate, and coconut coir and answer two science questions. First, what is the potential for copper removal and recovery using strong acids as a desorbing agent? Second, how does the adsorptive capacity of the sorption media vary through multiple adsorption/desorption cycles?

2. Methods and materials

2.1. Adsorption tests

Batch adsorption tests were carried out to produce copper-loaded media with which to conduct the desorption tests. The tests were conducted using 300 mL distilled water spiked with Fisher Scientific 1000 ppm copper standard (copper nitrate). Varying copper solution concentrations of 0.2, 0.6, 1.0, 2.0, and 3.0 $mg \cdot L^{-1}$ were added to 500 mL flasks containing 50 g of expanded clay and tire chunk, 30 g of media mixture, and 10 g of coconut coir. The flasks were then mixed thoroughly for 30 and 60 min on a New Brunswick Scientific *Excella E2* shaking platform at 200 rpm and covered with parafilm to avoid external disturbances. After mixing, the solution was extracted from the flasks, filtered through a 0.45 μm filter, and analyzed in triplicate using the United States Environmental Protection Agency (USEPA) Bicinchoninate Method no. 8506 and a HACH DR 2800 spectrophotometer. In all tests, the temperature was kept at 23 °C ± 3.0 °C, and the pH was adjusted to 3.75 ± 0.1 using $HCl_{(aq)}$.

2.2. Screening of desorbing agents

Desorption tests with 4 different desorbing agents were carried out on the copper-loaded media in contact with adsorbate solution for 60 min at a pH of 3.85. The selected desorbing agents were DI water, 0.1 M HCl, 0.1 M HNO_3, and 0.1 M H_2SO_4. For each desorbing agent, duplicates of 5 g media mixture, tire chunk, and expanded clay, and 1 g of the coconut coir were exposed to 30 mL of desorbing solution for 180 min on a shaking platform at 200 rpm. All media were oven-dried at 75 °C for a minimum of 36 h prior to the test. After mixing, the solution was extracted from the flasks, adjusted to a pH between 4 and 6 using 5.0 N KaOH, filtered through a 0.45 μm filter, and analyzed individually using the USEPA Bicinchoninate Method no. 8506.

Relative desorption strength among the 4 desorbing agents was evaluated using the desorption efficiency as the common indicator, defined below:

$$Desorption\ Efficiency = \frac{C_e V}{q_{0D} m} \times 100\% \quad (1)$$

where q_{0D} is the solid-phase copper concentration ($mg \cdot g^{-1}$) before desorption, m is the mass of media (g), C_e ($mg \cdot L^{-1}$) is the liquid-phase copper concentration in the desorbing solution, and V (L) is the volume of desorbing solution.

Batch desorption tests were conducted on media in contact with adsorbate solution for 30 min with 300 mL 0.1 M HCl as the desorbing agent. The desorbing agent was added to 500 mL flasks containing 50 g of expanded clay and tire chunk, 30 g of media mixture, and 10 g of coconut coir. The flasks were then mixed thoroughly for 30 min on a shaking platform at 200 rpm.

2.3. Desorption equilibria

Batch desorption tests were carried out on the media to establish the equilibrium desorption isotherms for the media mixture and individual media. Data from the batch desorption tests were fit to both the Freundlich and Langmuir equations for desorption isotherms:

$$q = K_{f,D} C_{e,D}^{1/n} \quad (2)$$

$$q = q_{max,D} \frac{K_{L,D} C_{e,D}}{1 + K_{L,D} C_{e,D}} \quad (3)$$

where q is the solid-phase copper concentration ($mg \cdot g^{-1}$), $C_{e,D,}$ ($mg \cdot L^{-1}$) is the copper concentration in the desorbing solution, $K_{f,,D}$ ($mg \cdot g^{-1}$) is the Freundlich desorption coefficient, n (dimensionless) is the nonlinearity factor, $K_{L,D}$ ($mg \cdot L^{-1}$) is the Langmuir desorption coefficient, and $q_{max,D}$ ($mg \cdot g^{-1}$) for the desorption isotherm an indicator of the desorption capacity of the sorbent–desorbate system. The Freundlich and Langmuir isotherm parameters for adsorption and desorption were optimized by minimizing root mean squared error (RMSE) between the experimental data and the predicted isotherm equation.

2.4. Desorption kinetics

The kinetics of the desorption reaction were observed experimentally and fit to both the classical rate-law kinetic equations and the Lagergren kinetic equations for sorption. The rate law kinetic equations were adapted for desorption reactions by assuming that the adsorbed copper concentration, $q(t)$ is related to the initial adsorbed copper concentration, q_0, by a reaction rate coefficient, k. The data was fit to both first- and second-order kinetic equations by minimizing the sum of the squared error between the kinetic desorption data and the model. For first-order kinetics, the kinetic equation takes the form:

$$q = q_0 e^{-k_{1D} t} \quad (4)$$

where k_{1D} (min^{-1}) is the reaction rate constant and t is the reaction time. For second-order kinetics, the kinetic equation takes the form:

$$\frac{1}{q} = \frac{1}{q_0} + k_{2D} t \quad (5)$$

where the reaction rate constant, k_{2D} is in units of g mg^{-1} min^{-1}.

The Lagergren pseudo first- and pseudo-second order kinetic equations can be adapted for desorption by assuming that the rate of desorption is proportional to the number of metal-filled sites and the square of the number of metal-filled sites, respectively (Njikam and Schiewer, 2012). The pseudo first-order kinetic equation is given as:

$$q_D = q_{0D}\left(1 - e^{-k_{P1D}t}\right) \tag{6}$$

where q_{0D} ($mg \cdot g^{-1}$) is the amount of desorbed copper at desorption equilibrium, q_D ($mg \cdot g^{-1}$) is the amount of copper that has been desorbed, and k_{P1D} is the reaction rate constant (min^{-1}) for the pseudo first- order desorption reaction. The pseudo second order kinetic equation is given as:

$$q_D = \frac{{q_{0D}}^2 \cdot k_{P2D} \cdot t}{1 + k_{P2D} \cdot q_{0D} \cdot t} \tag{7}$$

where k_{P2D} is the reaction rate constant ($g \cdot mg^{-1} \cdot min^{-1}$) for the pseudo second-order desorption reaction. Desorption kinetic data were obtained by exposing 500 mL flasks containing 50 g of expanded clay and tire chunk, 30 g of media mixture, and 10 g of coconut coir to 300 mL of 0.1 M HCl. Samples were taken at predetermined times and analyzed using the methods presented in Section 2.1.

2.5. Adsorption and desorption cycles

Re-use of sorption media through multiple sorption–desorption cycles inevitably results in a decrease in performance per each cycle in terms of total metal ion removal. A reduction in the number of available sorption sites occurs due to incomplete desorption of cations undergoing reversible sorption reactions and the occurrence of non-reversible sorption reactions. Adsorption and desorption cycles were simulated by conducting batch experiments using the methods presented in Sections 2.1 and 2.2. For each media type, 5 flasks filled with a constant mass of adsorbent (50 g expanded clay and tire chunk, 30 g mixture, 10 g coconut coir) were exposed to 300 mL varying copper solution concentrations of 0.2, 0.6, 1.0, 2.0, and 3.0 $mg \cdot L^{-1}$ for 30 min. The media were then rinsed with about 300 mL of DI water and exposed to 300 mL of 0.1 M HCl for 30 min. After desorption batch tests, the media were rinsed again with about 300 mL of DI water. This process was completed for 3 cycles of adsorption/desorption. The change in adsorption performance between successive cycles may also be quantified by the ratio $K_{f,i+1}/K_{f,i}$, where i represents the number of adsorption/desorption cycles the media has undergone. In this case, a ratio of 1 implies no decrease in adsorption whereas a ratio less than 1 implies a decrease in adsorption.

2.6. Material imaging and analysis

All the raw, Cu-loaded after adsorption, and Cu-desorbed powder samples for coconut coir, expanded clay, tire chunk, and the media mixture were milled, ground, and passed through 300 mesh sieves before analysis. Crystalline structures of adsorbents for raw, Cu-loaded, and Cu-desorbed samples were measured by XRD scanned from 10 to 80° (2θ) with a scan rate of 4° (2θ) min^{-1} and monochromatic CuK_α radiation (MAC Science, MXP18) at 30 kV and 20 mA and further identified by a computer database system (Joint Committee on Powder Diffraction Standards (JCPDS)). The morphology, particle size distribution, and microstructure of raw, Cu-loaded, and Cu-desorbed samples were also determined using FE–SEM (Hitachi S–4700 II) with a resolution of 0.1 nm. The quantities of carbon, oxygen, sulfur, copper, aluminum, and silicon atoms in raw, Cu-loaded, and Cu-desorbed samples were identified using energy dispersion spectroscopy (EDS). The average copper metal contents in raw, Cu-loaded, and Cu-desorbed samples, were digested by 01 M $HCl/HF_{(aq)}$ and evaluated using both atomic absorption spectroscopy (AAS, GBC model 908) and induced couple plasma/mass spectroscopy (ICP/MS, ELAN model 5000). Each calibration curve was generated with its corresponding standard metal solution at 10 different concentrations to generate the expected Cu metal concentrations in the raw, Cu-loaded, and Cu-desorbed samples, respectively. Infrared spectra of the raw, Cu-loaded, and Cu-desorbed samples were prepared mixed with KBr in powder sample disks and were recorded and calculated on a Varian 1000 Digilab FTIR spectrometer of Attenuated Total Reflectance (ATR) with fully computerized data storage and data handling capabilities over the range of 4000–400 cm^{-1}. For all spectra reported, a 64-scan data accumulation was conducted at a resolution of 4 cm^{-1}.

3. Results and discussion

3.1. Screening of desorbing agents

Regeneration of the media was quite successful with the use of strong acids (Fig. 1), especially for hydrochloric acid, which provided 83%, 84%, and 48% desorption efficiencies for the expanded clay, coconut coir, and media mixture, respectively. The tire chunk exhibited a desorption efficiency of greater than 100% for HCl, which can be attributed to leaching of pre-existing copper content in the tire material from copper-containing brake dust and the tire manufacturing process. The success of strong acids as a desorbing agent points to ion exchange as the dominant sorption mechanism. Desorption under DI water was nearly negligible, however, which suggests only a small contribution from physical sorption toward the overall copper adsorption.

3.2. Equilibrium desorption isotherm

Data from batch desorption tests were fit to both the Langmuir and Freundlich isotherm equations, which both fit the desorption data reasonably well; however, the Freundlich equation resulted in a better prediction for all media types, particularly for the

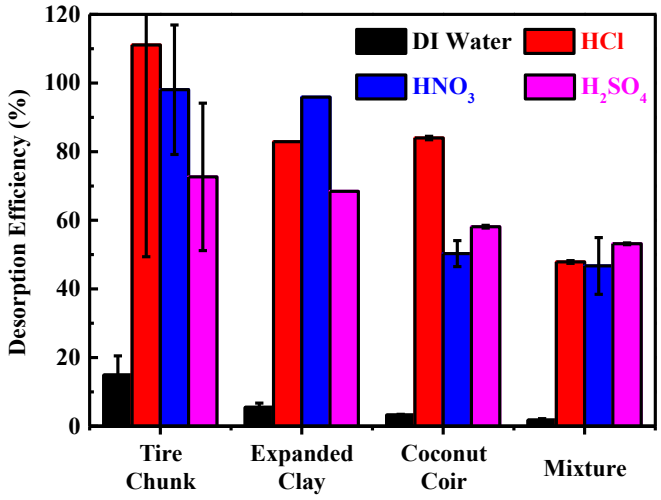

Fig. 1. Desorption efficiencies for each media type using DI water, 0.1 M hydrochloric acid, 0.1 M nitric acid, and 0.1 M sulfuric acid as desorbing agents at 23 °C.

expanded clay (Table 1). The Freundlich parameter K_f, which is also the slope of the desorption isotherm, indicates the relative strength, or effectiveness of the desorption process on the Cu-loaded media. The values for K_f (Table 1) indicate that the coconut coir, followed by the expanded clay and the media mixture, experienced the strongest desorption, which is consistent with findings shown in Fig. 1. Note that all of the Freundlich nonlinearity parameters (n) are significantly less than 1, which corresponds to concave-type isotherms (Fig. 2). This finding is in contrast to the convex-type isotherms typically observed for adsorption data (Cox et al., 1997), suggesting that desorption efficiency decreases as the amount of initial adsorbed copper increases, resulting in a highly nonlinear, concave isotherm.

For all media types, a desorption efficiency greater than 100% was observed for media exposed to copper adsorbate of the lowest concentration (0.2 mg·L^{-1}). As a result, a shift factor was applied to the desorption data to provide positive values of q for model fitting. Although this was mathematically necessary, it did introduce a small amount of error in the modeling effort. The modeling results for the tire chunk are not shown because the existing copper content in the material skewed the results over the entire range of initial Cu adsorbate concentrations.

3.3. Desorption kinetics

The kinetic data revealed that the desorption reaction was rapid, with more than 50% of desorption occurring within the first 30 s for all media types. Equilibrium was reached within 30 min, with the exception of the tire chunk. For the rate law kinetic equations, a decrease in correlation was observed as the desorption efficiency decreased (Table 2), which can be attributed to the mathematical structure because it predicts that the remaining sorbed metal goes to zero as t goes to infinity. With less than 100% desorption, the remaining sorbed metal, q_{0D} actually approaches an asymptotic value. For the Lagergren first- and second-order kinetic equations, however, q_{0D} was assumed to be a model parameter, the amount of desorbed copper (mg·g^{-1}) at equilibrium, instead of a variable, the total amount of initial sorbed copper. (mg·g^{-1}). As a result of this assumption, strong corellation was observed with kinetic data for both pseudo first- and second-order reaction models, with R^2 values all above 0.96. The exception was the tire chunk, which exhibited typical kinetic characteristics for the first 10 min, with a slower reaction occurring after that (Fig. 3), most likely attributable to desorption of the sorbed copper within the first 10 min, followed by the slow release of the pre-existing copper content in the tire chunk (Table 3).

3.4. Adsorption and desorption cycles

Three successive adsorption/desorption cycles were carried out on each media type as a batch system with initial copper concentrations ranging from 0.2 to 3.0 mg·L^{-1}. The results showed that the reusability of the media is impacted after just 3 cycles. The sorption of copper on the media decreased by 44%, 100%, 74%, and 19% for the media mixture, tire chunk, expanded clay, and coconut coir,

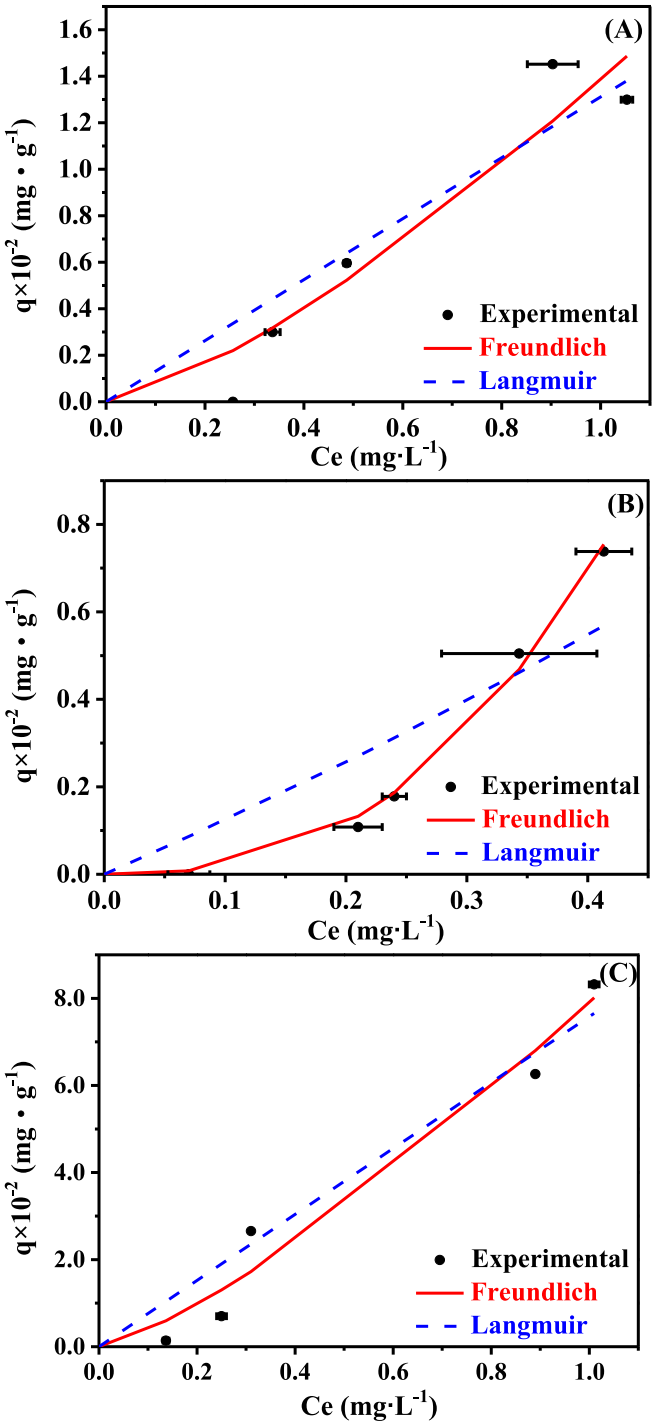

Fig. 2. Desorption isotherms of (A) media mixture (B) expanded clay, and (C) coconut coir at 23 °C.

Table 1
Summary of desorption isotherm parameters at 23 °C.

Media	Langmuir isotherm			Freundlich isotherm		
	K_L (mg·L^{-1})	q_{max} (mg·g^{-1})	RMSE (mg·g^{-1})	K_f (mg·g^{-1})	n	RMSE (mg·g^{-1})
Mixture	0.00217	6.040	0.00207	0.0139	0.741	0.001730
Expanded clay	−0.29300	−0.041	0.00128	0.0730	0.389	0.000216
Coconut coir	0.00478	15.929	0.00778	0.0791	0.769	0.006030

Table 2
Summary of Lagergren kinetic model parameters at 23 °C.

Media	Lagergren pseudo first-order			Lagergren pseudo second-order		
	K_{P1D} (min^{-1})	q_{0D} ($mg \cdot g^{-1}$)	R^2	K_{P2D} (min^{-1})	q_{0D} ($mg \cdot g^{-1}$)	R^2
Mixture	1.39	0.0195	0.959	136	0.0204	0.985
Tire chunk	1.35	0.00370	0.751	651	0.00388	0.849
Clay	2.49	0.0105	0.977	464	0.0109	0.994
Coconut coir	2.27	0.0515	0.977	82.5	0.0535	0.989

Table 3
Summary of rate law kinetic model parameters. Note the tire chunk parameters are not included because observed desorption was greater than 100% due to pre-existing copper content.

Media	q_0 ($mg \cdot g^{-1}$)	q_{0D} ($mg \cdot g^{-1}$)	Desorption efficiency (%)	R^2 (1st-order)	R^2 (2nd-order)
Mixture	0.0234	0.0204	87.2	0.894	0.948
Expanded clay	0.0126	0.0109	86.5	0.917	0.934
Coconut coir	0.0814	0.0535	65.7	0.657	0.689

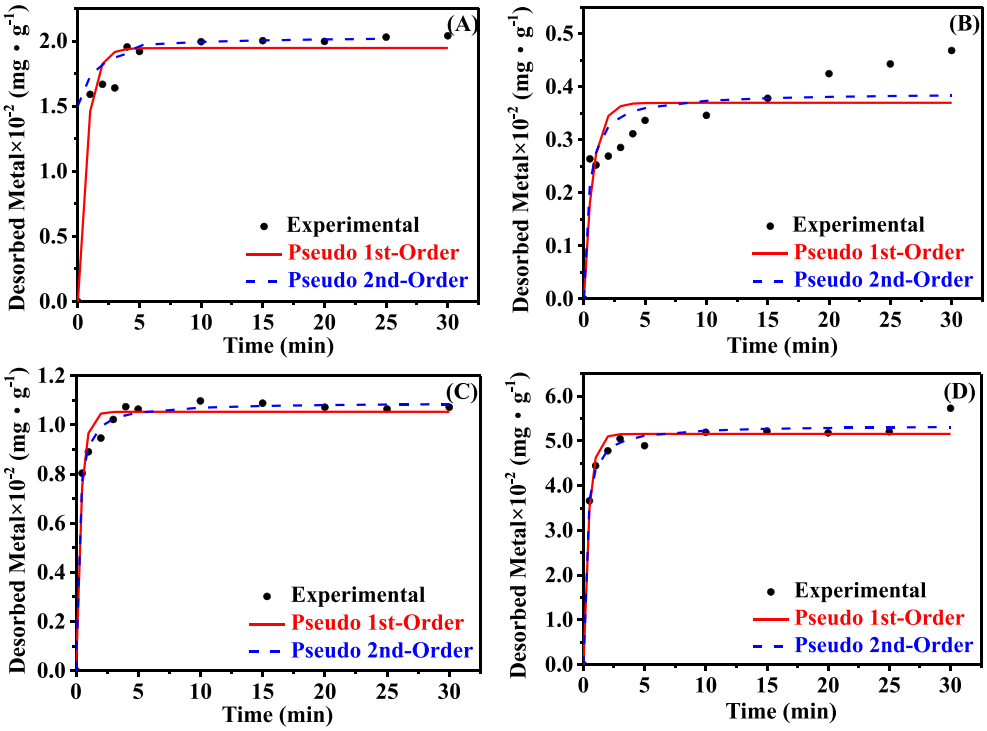

Fig. 3. Desorption kinetics of (A) media mixture (B) tire chunk (C) expanded clay aggregate, and (D) coconut coir at 23 °C.

respectively, based on the media with an initial sorbate concentration of 3.0 $mg \cdot L^{-1}$. Fig. 4 shows a steep decrease in adsorption for expanded clay between the first and second cycles, whereas the decrease is more gradual for the other media types, indicating that expanded clay would only serve one useful life cycle if used in isolation. The Freundlich adsorption parameters (Table 4) for the successive cycles give further description to the observed decrease in adsorption over multiple cycles. The biggest decrease in adsorption capacity was observed for the expanded clay between the first and second cycles, whereas the coconut coir adsorption was the least impacted by the desorption stage.

3.5. Material imaging and analysis

The FE-SEM microphotographs (Fig. 5) were used to investigate the morphologies, crystallinity, and microstructures of the raw (A), Cu-loaded (B), and Cu-desorbed (C) samples consisting of the media mixture, tire chunk, expanded clay, and coconut coir materials, respectively. The adsorption media mixture mixed with 1:1:1 vol ratio of tire chunk, expanded clay, and coconut coir has an irregular shape with average diameters of approximately 0.5–15 μm (Fig. 5A-(a)). Similarly, the particle size of Cu-loaded/Cu-desorbed media mixture was around 1–8 μm, as identified by the FE-SEM micrograph (Fig. 5B, C-(a)). The media mixture was well dispersed with irregular shapes and sizes after the adsorption/desorption removal process of copper contaminants. Milled or ground tire chunk after a pretreatment process has 60–90 nm in diameter and 150–350 nm in length ultrafine particles, well-dispersed on the surface of pretreated tire chunk (Fig. 5A-(b)). Additionally, aggregated ultrafine ZnO particles or carbon black powders may be reformed by heat effects in the process of milling or grinding. After the adsorptive removal and desorption processes

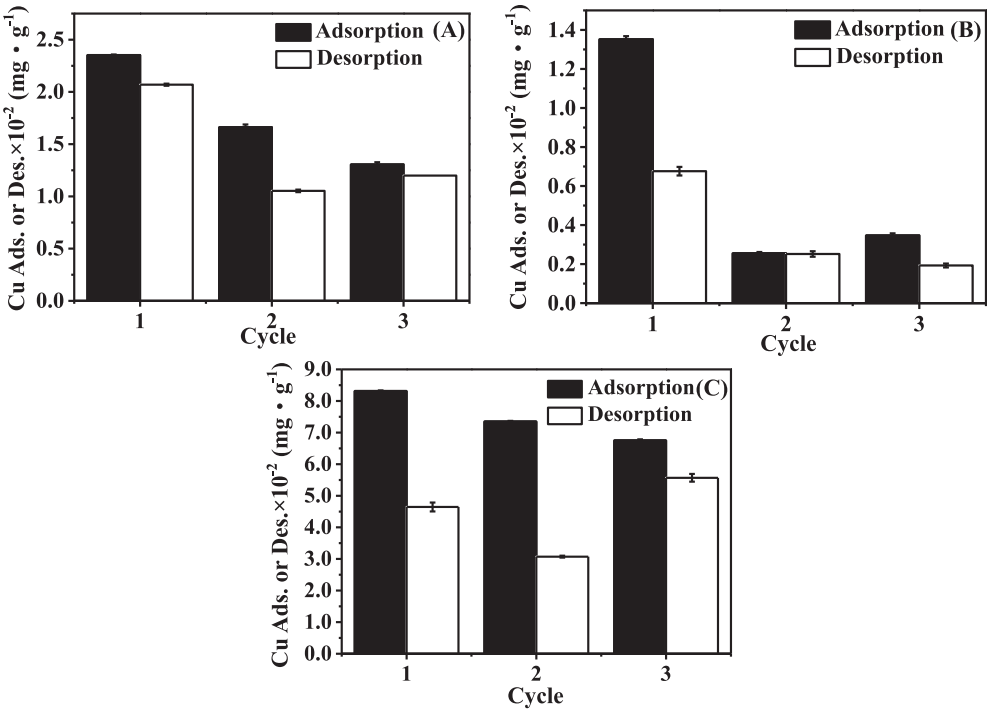

Fig. 4. 3 cycles of adsorption/desorption data for (A) media mixture (B) expanded clay aggregate, and (C) coconut coir at 23 °C.

Table 4
Summary of Freundlich adsorption coefficient ratios for 3 adsorption/desorption cycles. Subscripts 1, 2, and 3 refer to the respective adsorption/desorption cycle at 23 °C.

Media	$K_{f,2}/K_{f,1}$	$K_{f,3}/K_{f,2}$
Mixture	0.617	1.045
Exp. clay	0.222	0.853
Coconut coir	0.795	0.989

of copper-contaminated wastewaters, it was also well-dispersed with irregular shapes and sizes around 1–12 μm identified by FE–SEM micrograph (Fig. 5B,C-(b)). Interestingly, there are no structural changes or damages between adsorption/desorption processes of copper-contaminated wastewaters onto tire chunk using 0.1 M HCl as a desorbing agent (Fig. 5A).

According to the FE-SEM microphotos, significant morphological differences exist between the raw expanded clay and Cu-loaded/Cu-desorbed expanded clays after the adsorptive removal process of copper-contaminated stormwater (Fig. 5A-(c), 5B-(c) and 5C-(c)), respectively. Irregular shapes of crystals and notably aggregated ultrafine particles around 2–10 μm diameter of SiO_2 mixed with Al_2O_3 green adsorbents were observed (Fig. 5A-(c)). The Cu-loaded/Cu-desorbed expanded clays were well dispersed with irregular shapes and sizes around 0.5–10 μm (Fig. 5B-(c) and 5C-(c)). Furthermore, FE-SEM analyses reveal that the SiO_2/Al_2O_3 ultrafine particles are highly mixed and dispersed, and, interestingly, also show that the ultrafine particle sizes of SiO_2/Al_2O_3 mixtures were not all separated, but rather were narrowly distributed, which might result from van der Waals' force attraction of the ultrafine particles. The rough surface of coconut coir material is thus favorable for adsorptive removal of copper (Fig. 5A-(d)), consistent with the result of the EDS measurements (Table 5). In addition, notably visualized spherical or irregular-shaped CuO ultrafine particles with a diameter of approximately 100–250 nm were found (Fig. 5 B-(d)). The CuO ultrafine particles were possibly digested and washed out from the surface of pore structures in the desorption process using 0.1 M HCl (Fig. 5C-(d)).

Powder X-ray diffraction analyses of the porous adsorption materials were performed to confirm the crystalline phases in the media mixture, tire chunk, expanded clay, and coconut coir materials. Plots of the XRD patterns of raw and Cu-loaded/Cu-desorbed media mixture and expanded clay Fig. 6(A) and 6(C), respectively, show that both raw and Cu-loaded/Cu-desorbed expanded clay is crystalline, indicated by sharp diffraction peaks. The intensive peaks appearing at 2θ angles in the XRD patterns of raw and Cu-loaded expanded clay are characteristics of crystalline materials, and the fine structure remains stable and similar after the copper adsorption/desorption processes. We observed that the diffraction peaks for both raw and Cu-loaded/Cu-desorbed expanded clay corresponded to hexagonal-typed SiO_2 of (100), (011), (110), (112), (121), (440) (JCPDS file No.74-1811) and monoclinic-typed Al_2O_3 of (400), (310), (511), (113) (JCPDS file No. 86-1410) as well the peaks for the raw and Cu-loaded/Cu-desorbed media mixture. Based on the intensities of XRD patterns of raw and Cu-loaded/Cu-desorbed mixture or expanded clay, the major component appears to be SiO_2. Both raw and Cu-loaded/Cu-desorbed samples are crystalline, evidenced by their sharp diffraction peaks, and the position and relative intensity of the diffraction peaks of the samples match well with the standard XRD data for hexagonal-typed SiO_2 and monoclinic-typed Al_2O_3. Moreover, the intensive peaks appearing at 2θ angles in the XRD pattern of hexagonal-typed SiO_2 and monoclinic-typed Al_2O_3 are characteristics of these materials, which possess numerous pores or cavities where copper species can be easily exchanged on the surface. The average crystallite size of expanded clay is calculated to be 150–250 nm using the Scherrer formula from the hexagonal-typed SiO_2 (011) plane (which corresponds the strongest peak). There clearly are no structural changes or damages between the adsorption and desorption processes of copper-contaminated wastewaters onto expanded clay/media mixture using 0.1 M HCl as a desorbing agent (Fig. 6(A) and 6(C), respectively).

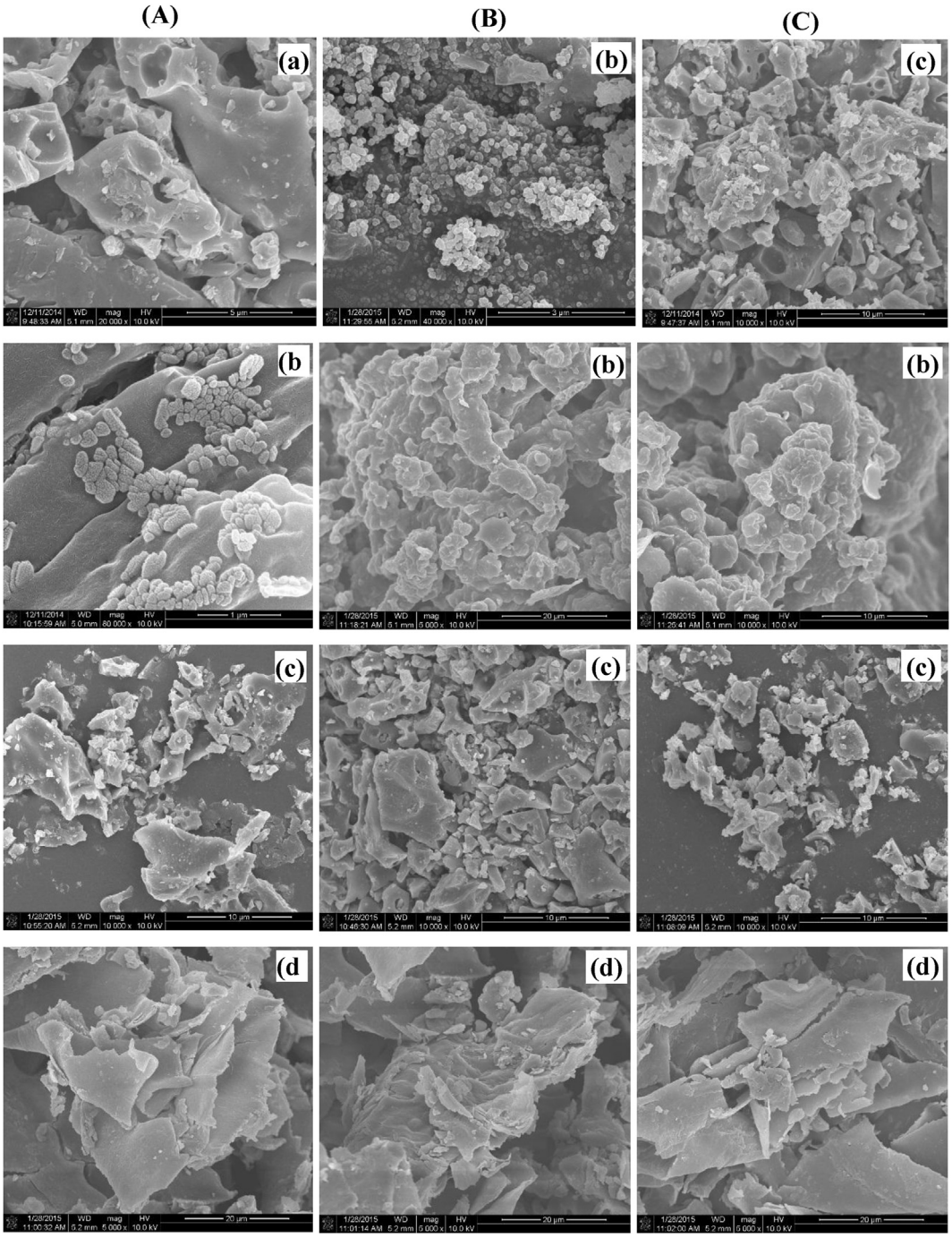

Fig. 5. FE-SEM micrographs of (A) raw, (B) Cu-adsorbed, and (C) Cu-desorbed powder samples for (a) media mixture, (b) tire chunk, (c) clay, and (d) coconut coir green adsorption media.

The XRD patterns of raw and Cu-loaded/Cu-desorbed tire chunk and coconut coir adsorption media (Fig. 6(B) and 6(D), respectively), show a broad and less intensive peak around $2\theta = 20–22^{\circ}$, which can be attributed to the graphitic structure of activated carbons generated from pretreated tire chunk and coconut coir wastes. The observed 2θ angles are also characteristics of micro- or meso-porous materials of tire chunk and coconut coir, which possess numerous tiny pores or cavities. With the additives of sulfur and ZnO, which improve the hardness and abrasion of tires, bonded ZnS and ZnO particles were observed in the framework of the tire chunk. In addition, the other 11 peaks could be indexed to the (100), (101) of hexagonal-typed ZnS (JCPDS file No.80-0007), (100), (002), (101), (102), (110), (103), (112) of hexagonal-typed ZnO (JCPDS file No. 36-1451) and (111), (022) planes of monoclinic-typed CuO particles (JCPDS file No.48-1548), respectively. The calculated mean particle size of the loaded ZnS, ZnO, and CuO particles by Scherrer equation were about 115, 155, and 130 nm, which corresponds to the strongest peak of (100), (101), or (111), respectively.

Results suggest that CuO was finely dispersed on the surface of coconut coir and that after pretreatment there were not enough enhancements in the crystal and pore structures (Fig. 6(D));

Table 5
Ultimate analyses of raw, Cu-loaded after adsorption, and Cu-desorbed powder samples for media mixture, tire chunk, expanded clay, and coconut coir using average values of EDS/ICP-MS/AA, respectively (variation of ±0.03 atom%).

Adsorbent	Carbon (atom%)	Oxygen (atom%)	Aluminum (atom%)	Silicon (atom%)	Copper (atom%)	Sulfur (atom%)
Mixture						
Raw (fresh)	30.31	42.42	6.69	20.03	N.A.	0.55
Cu-loaded	30.46	42.36	6.82	19.90	0.04	0.42
Cu-desorbed	30.30	42.48	6.67	20.01	0.02	0.52
Expanded clay						
Raw (fresh)	N.A.	45.68	11.66	42.66	N.A.	N.A.
Cu-loaded	N.A.	45.52	11.29	43.10	<0.01	N.A.
Cu-desorbed	N.A.	47.59	10.93	41.48	N.A.	N.A.
Tire chunk						
Raw (fresh)	83.80	13.37	N.A.	N.A.	N.A.	2.83
Cu-loaded	83.79	13.36	N.A.	N.A.	<0.01	2.82
Cu-desorbed	83.56	13.77	N.A.	N.A.	N.A.	2.67
Coconut coir						
Raw (fresh)	66.79	33.21	N.A.	N.A.	N.A.	N.A.
Cu-loaded	65.86	33.33	N.A.	N.A.	2.81	N.A.
Cu-desorbed	65.14	34.01	N.A.	N.A.	0.85	N.A.

Note: "N.A." denotes "not available".

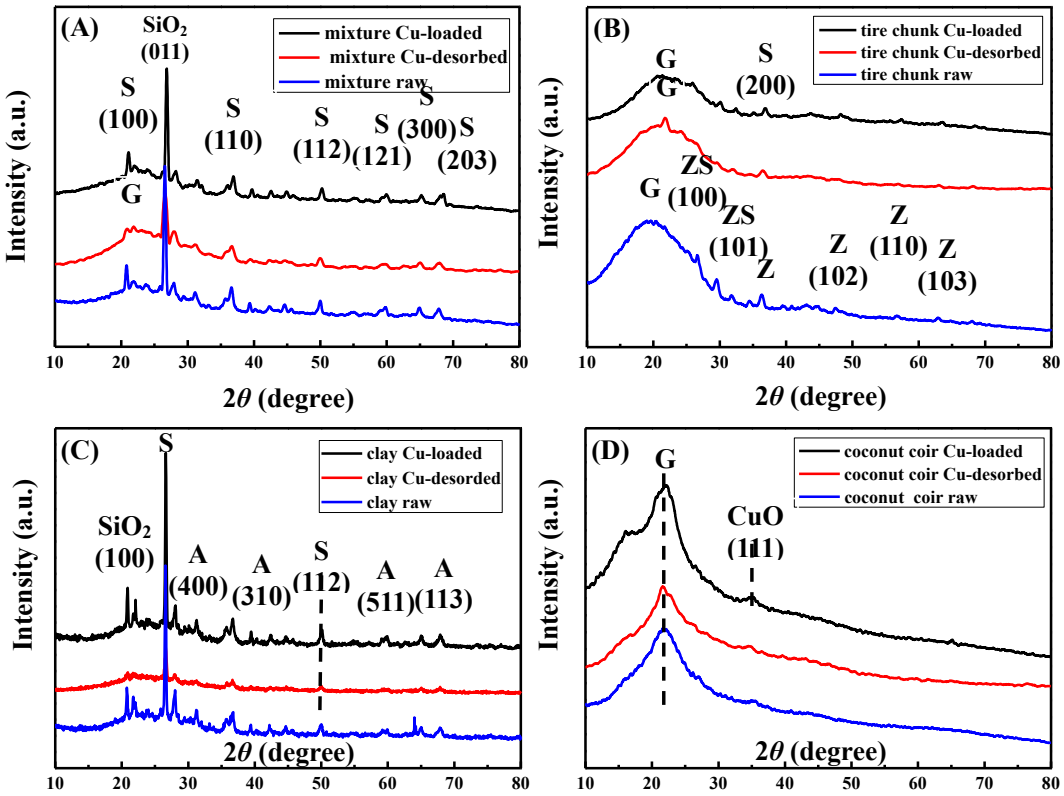

Fig. 6. XRD patterns of (A) media mixture (S: SiO_2; A: Al_2O_3), (B) tire chunk (G: graphite; ZS: ZnS; Z: ZnO), (C) expanded clay (S: SiO_2; A: Al_2O_3), and (D) coconut coir (G: graphite) for the raw, Cu-loaded or Cu-desorbed samples.

however, these findings indicate that CuO particles in as-synthesized Cu-loaded coconut coir were not highly crystalline and ultrapure. Interestingly, the samples were pretreated under lower milling and grinding temperatures, and thus Cu_2O or CuS by-products should not be formed. As such, the diffraction peaks cannot categorically reveal the existence of Cu_2O or CuS peaks. All the pretreated samples indicate similar diffraction lines and intensities at identical 2θ values. The copper species exchanged in pretreated coconut coir was confirmed by the XRD pattern (Fig. 6(D)), and the residue was CuO mixed onto the surface of coconut coir. XRD also showed that the CuO ultrafine particles were possibly digested and washed out from the surface of pore structures in the desorption process. These results are consistent with the data of FE-SEM microphotos (Fig. 6(D)).

Generally, FTIR can provide the chemical properties of organic functional groups on the surface of media mixture, tire chunk, expanded clay, and coconut coir for the raw, Cu-loaded or Cu-desorbed samples. Based on the media mixture containing tire chunk, expanded clay, and coconut coir, the specific functional groups such as S—H, O—H, C═O were found (Fig. 7(A)). Because the tire chunk composites are generally mixed with the additives of sulfur powders, which can improve the hardness and abrasion of

tires, S–H and C=S bonding were observed in the framework of the tire chunk (Fig. 7(B)). From the XRD patterns of expanded clays (Fig. 6(C)), hexagonal-typed SiO_2 and monoclinic-typed Al_2O_3 are characteristics of these materials, and Si–O and Al–O bonds were found on the surface of expanded clays (Fig. 7(C)). Based on the porous and amorphous properties of coconut coir, the moisture and organic functional groups such as O–H, C=O, C–H bonding were observed (Fig. 7(D)). Notably, no significant changes were observed on the surface during adsorption/desorption processes of Cu-contaminated wastewaters onto coconut coir samples using HCl as a desorbing agent (Fig. 7).

The results of elemental analyses of the media mixture, tire chunk, expanded clay, and coconut coir by using average values of EDS/ICP-MS/AA, respectively, show that carbon constituents are the main component of typical tire chunk and coconut coir adsorbents (Table 5). Low metal species and high sulfur content in tire chunk and mixture are also notably found. Moreover, silicon and oxygen are the main components in the expanded clay adsorbent, and trace copper species are present in both Cu-loaded expanded clay and tire chunk adsorbents, respectively. By contrast, the Cu contents in Cu-loaded mixture and coconut coir adsorbents are 0.4 and 2.81% (atom), respectively. The copper species are loaded or bonded on the hydrophilic surface of coconut coir due to the combination of ion exchange with –OH and –COO functional groups and electrostatic attraction onto a higher specific surface area (Li et al., 2015; Acheampong et al., 2011). Based on the electrostatic attraction (e.g., –OH) and ion exchange effects, expanded clay adsorbents have shown that copper sorption occurs in the process of adsorption. Similarly, tire chunk adsorbents also have trace adsorption capacities, and sorption occurs primarily through ion exchange or possibly bonding with sulfur atoms (Cu–S) on the hydrophobic surface of the adsorbent framework (Calisir et al., 2009). In addition, the higher concentration of copper loaded in the coconut coir correlates with the higher porosity and void ratio compared with the other adsorbents. Conversely, the concentration of copper species in tire chunk is lower compared with that of mixture adsorbents due to the effects of lower porosity and void ratio. In the desorption process, the media mixture and coconut coir still have copper contaminated residues in the frame structures that may not be removed during the desorption procedures. These results are consistent with our data (Fig. 1). Comparing the copper adsorption and desorption processes, different desorbing agents of DI water, HCl, HNO_3, and H_2SO_4 are also likely a dominant factor here, based on at least two possibilities: (1) acidic desorption agents may remove and leach out the Cu-contaminants inside or bonded with the surface of these green adsorbents; (2) the hydrophobic or hydrophilic surface properties of the green adsorbents may affect the wetting abilities of the surface for removing copper contaminant. Based on the comparison in Table 5, increasing percentages of oxygen atoms and decreasing copper, silicon, aluminum, or sulfur atoms during the desorption process using acidic desorption agents were found. Acidic desorption agents are generally suggested to be more suitable for application on the desorption processes of copper-contaminated wastewaters.

4. Conclusions

A green sorption media mixture composed of recycled tire chunk, expanded clay aggregate, and coconut coir was evaluated for its desorption characteristics. Screening of potential desorbing agents showed that the use of HCl as a desorbing agent had the greatest potential. Batch equilibrium tests using 0.1 M HCl revealed

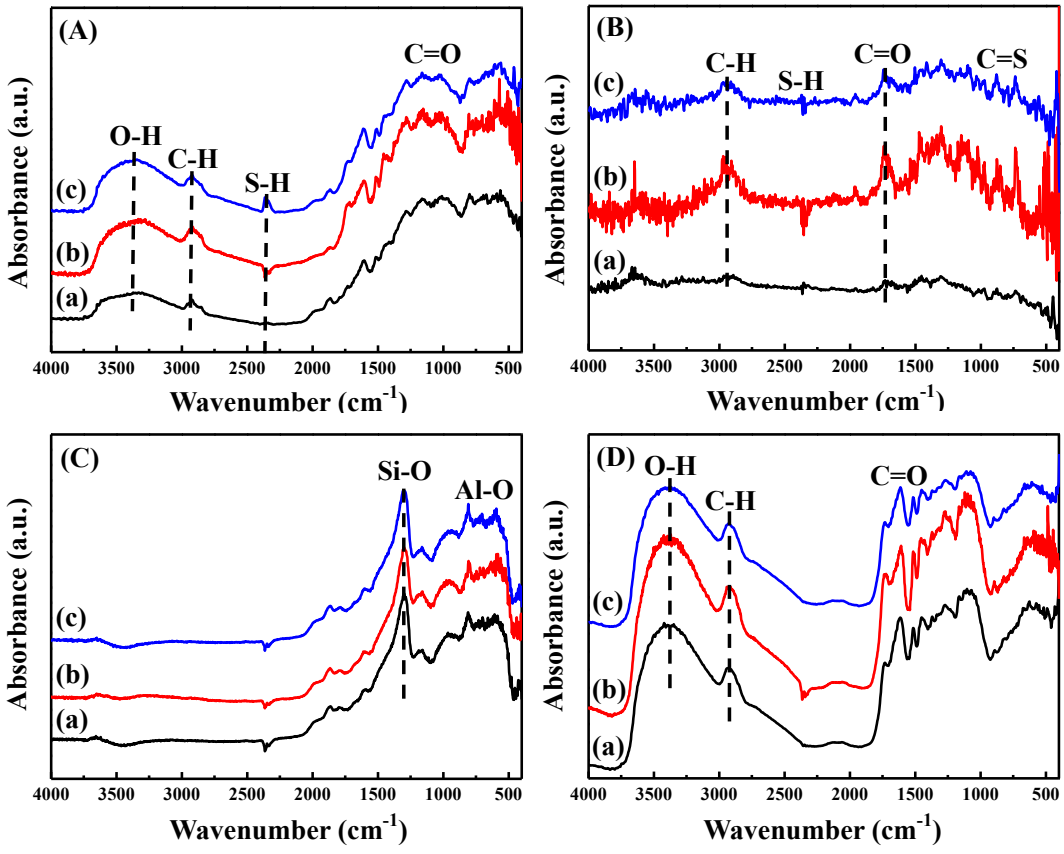

Fig. 7. FTIR absorbance spectra of (a) raw (fresh), (b) Cu-Loaded, and (c) Cu-desorbed samples for (A) media mixture (B) tire chunk, (C) expanded clays, and (D) coconut coir.

a Freundlich-type desorption isotherm, which was highly nonlinear and concave in nature. Kinetic desorption tests found that the Lagergren pseudo second-order kinetic model best described the data with more than 50% of desorption occurring within 30 s. Batch adsorption and desorption was carried out over 3 cycles, showing that the tire chunk and expanded clay experience severely decreased adsorption by the third cycle, whereas the media mixture and coconut coir exhibited only a modest decrease in adsorption over the 3 cycles. FE-SEM imaging and XRD analyses revealed primarily surface sorption of CuO species onto the coconut coir, which were digested and washed out during the desorption process. EDS measurements confirmed the successful, but incomplete, desorption from Cu-loaded media mixture and coconut coir. Regeneration through the use of strong acids as a desorbing agent confirms application potential. Overall, the media can serve multiple life cycles, which can be disposed as untreated non-hazardous waste at the end of its life cycle, and the adsorbed copper can be recovered via metal hydroxide precipitation, generating little waste.

References

Acheampong, M.A., Pereira, J., Meulepas, R., Lens, P., 2011. Biosorption of Cu(II) onto agricultural materials from tropical regions. J. Chem. Technol. Biotechnol. 86, 1184–1194.

Al-Zoubi, H., Rieger, A., Steinberger, P., Pelz, W., Hasender, R., Hartel, G., 2010. Nanofiltration of acid mine drainage. Desalinization Water Treat 21, 148–161.

Calisir, F., Roman, F.R., Alamo, L., Perales, O., Arocha, M.A., Akman, S., 2009. Removal of Cu(II) from aqueous solutions by recycled tire rubber. Desalinisation 249, 515–518.

Chang, N.B., Marimon, Z.A., Xuan, Z., Vannah, B., Jones, J., 2014. System dynamics modeling for nitrogen removal in a subtropical stormwater wet pond. In: Chapter 17 in Ecological Modelling and Engineering of Lakes and Wetlands, Jørgensen. Elsevier, Amsterdam, The Netherlands.

Chen, T., Yan, B., Lei, C., Xiao, X., 2014. Pollution control and metal resource recovery for acid mine drainage. Hydrometallurgy 147–148, 112–119.

Cox, L., Koskinen, W., Yen, P.Y., 1997. Sorption-desorption of imidacloprid and its metabolites on soils. J. Agric. Food Chem. 45, 1468–1472.

Davis, A.P., Shokouhian, M., Ni, S., 2001. Loading estimates of lead, copper, cadmium, and zinc in urban runoff from specific sources. Chemosphere 44, 997–1009.

Dean, C.M., Sansalone, J.J., Cartledge, F.K., Pardue, J.H., 2005. Influence of hydrology on rainfall-runoff metal element speciation. J. Environ. Eng. 131, 632–642.

Febrianto, J., Kosasih, A., Sunarso, J., Ju, Y.H., Indraswati, N., Ismadji, S., 2009. Equilibrium and kinetic studies in adsorption of heavy metals using biosorbent: a summary of recent studies. J. Hazard. Mater. 162, 616–645.

Graves, G.A., Wan, Y., Fike, D., 2004. .Water quality characteristics of storm water from major land uses in South Florida. J. Am. Water Resour. Assoc. (JAWRA) 40, 1405–1419.

Hoang, T.C., Schneider, L., Rogevich, E., Bachman, P., Rand, G., Frakes, R., 2009. Copper release, speciation, and toxicity following multiple floodings of copper-enriched agricultural soils: implications in Everglades restoration. Water Air Soil Pollut. 199, 79–93.

Hilliges, R., Schriewer, A., Helmreich, B., 2013. A three-stage treatment system for highly polluted urban road runoff. J. Environ. Manag. 128, 306–312.

Kayhanian, M., Singh, A., Suverkropp, C., Borroum, S., 2003. Impact of annual average daily traffic on highway runoff pollutant concentrations. J. Environ. Eng. 129, 975–990.

Li, Z., Ge, Y., Wan, L., 2015. Fabrication of a green porous lignin-based sphere for the removal of lead ions from aqueous media. J. Hazard. Mater. 285, 77–83.

Mullett, M., Fornarelli, R., Raplh, D., 2014. Nanofiltration of mine water: impact of feed pH and membrane charge on resource recovery and water discharge. Membranes 4, 163–180.

Nason, J.A., Bloomquist, D.J., Sprick, M.S., 2012. Factors influencing dissolved copper concentrations in Oregon highway storm water runoff. J. Environ. Eng. 138, 734–742.

Njikam, E., Schiewer, S., 2012. Optimization and kinetic modeling of cadmium desorption from citrus peels: a process for biosorbent regeneration. J. Hazard Mater. 213–214, 242–248.

Pitt, R., Maestre, A., Hyche, H., Togawa, N., 2008. The updated stormwater quality database (NSQD) version 3. Proc. Water Environ. Fed. 16, 1007–1026.

Piwowarczyk, A., Holden, N., 2011. Adsorption and desorption isotherms of the nonpolar fungicide chlorothalonil in a range of temperate maritime agricultural soils. Water Air Soil Pollut. 223, 3975–3985.

Singh, A., Kumar, D., Gaur, J.P., 2008. Removal of Cu(II) and Pb(II) by *Pithophora oedogonia*: sorption, desorption, and the repeated use of the biomass. J. Hazard Mater. 152, 1011–1019.

Tassist, A., Lounici, H., Belhocine, D., Khelifa, A., Mameri, N., 2009. Removal and recovery of copper from aqueous solutions by *Streptomyces rimosus* biomass: enhancement of regeneration by desorption-electrolysis coupling. Desalinization Water Treat. 3, 210–216.

United States Environmental Protection Agency (USEPA), 2014. Water Quality Assessment and Total Maximum Daily Loads Information. http://www.epa.gov/waters/ir/index.html.

Vilar, V., Botelho, C., Boaventura, R., 2007. Copper desorption from *Geldium* algal biomass. Water Res. 41, 1569–1579.

Xie, Y., Xu, Y., Yan, L., Yang, R., 2005. Recovery of nickel, copper and cobalt from low-grade Ni-Cu sulfide tailings. Hydrometallurgy 80, 54–58.

Zhang, Z.Y., Zhang, F.S., 2014. A green process for copper recovery from waste printed circuit boards. Adv. Mater. Process. 878, 374–379.